Thermal Boundary Resistance between GaN and Cubic Ice and THz Acoustic Attenuation Spectrum of Cubic Ice from Complex Acoustic Impedance Measurements

Pierre-Adrien Mante, Chien-Cheng Chen, and Yu-Chieh Wen

Department of Electrical Engineering and Graduate Institute of Photonics and Optoelectronics,
National Taiwan University, Taipei 10617, Taiwan

Jinn-Kong Sheu

Institute of Electro-Optical Science and Engineering and Advanced Optoelectronic Technology Center,
National Cheng Kung University, Tainan 70101, Taiwan

Chi-Kuang Sun[*]

Department of Electrical Engineering and Graduate Institute of Photonics and Optoelectronics,
National Taiwan University, Taipei 10617, Taiwan
Molecular Imaging Center, National Taiwan University, Taipei 10617, Taiwan
and Institute of Physics, Academia Sinica, Taipei 115, Taiwan

A phonon nanoscopy method, based on the picosecond ultrasonics technique, capable of studying the complex acoustic reflection coefficient at frequency up to 1 THz is proposed and demonstrated. By measuring the reflection coefficient at the same surface location at the interface between GaN and air, and between GaN and the material to characterize, we get access to the THz amplitude and phase spectra of the acoustic phonon reflection. The retrieval of both these pieces of information then allows the calculation of the attenuation in a wide range of frequency and gives new insight into the Kapitza anomaly. This method is then applied to cubic ice, and the measurements of the elastic properties, the phonon anharmonic decay spectrum up to 1 THz, as well as the measurements of the thermal phonon lifetime at 150 K are all achieved.

The sub-THz frequency range (0.1–1 THz) is critical for acoustic phonons. In this frequency range, numerous phenomena responsible for the low-temperature thermal behavior of solids are predicted. For instance, the Kapitza resistance or thermal boundary resistance, which is the resistance to heat flow at an interface, drops in this frequency range. At temperatures below 1 K, the heat transport at the interface is satisfactorily modeled by the acoustic mismatch model (AMM) [1,2]. At higher temperatures, where the dominant phonon modes carrying the heat have frequency of hundreds of gigahertz, this model cannot explain the experimental observation [1,2]. Another interesting feature of this frequency range is the behavior of acoustic propagation attenuation. Attenuation at these frequencies is dominated by scattering with thermal phonons [3]. However, the usual thermal phonon lifetime (τ_{ph}) is in the range of a few picoseconds to subpicoseconds, so when the frequency becomes high ($\omega\tau_{ph} \gg 1$), this relaxation process saturates and three phonon processes become predominant [4–6]. In amorphous materials, the boson peak has been predicted to appear in this frequency range.

To study all these phenomena, a broadband source of acoustic phonons in the sub-THz range capable of working at variable temperature is needed. Concerning attenuation, inelastic light scattering techniques can study part of this range, but there is still a gap between the frequency attainable by Brillouin light scattering (up to a few hundred GHz) [7–9] and x-ray scattering (higher than 1 THz) [10]. The picosecond ultrasonics technique [11–15] can completely cover this frequency range and therefore has attracted lots of interest in recent years [12,15–17]. Usually, to study attenuation, one looks at the decrease of the amplitude of the acoustic signal after the propagation in the material. This technique has been successfully applied, but mostly at single frequency [18,19] and up to 0.7 THz [15,20].

In this Letter, we propose and demonstrate an experimental method enabling the study of both the amplitude and the phase of the acoustic reflection coefficient at an interface with frequency up to 1 THz, thanks to the broad generation and detection of the piezoelectric quantum well and the high interface quality. By measuring the complex acoustic reflection coefficient at an interface between a well-known material (GaN) and the material to be characterized, and at the same location but when the material is absent, we can retrieve the elastic and viscous properties of the material. We can then estimate the thermal boundary resistance and the attenuation spectrum. Contrary to methods based on the propagation of waves through the material to be characterized, in which the high-frequency components are strongly attenuated, our method, based on the reflection of acoustic waves, allows the study of the

attenuation frequency up to 1 THz. From the THz band-width attenuation spectrum, we are able to estimate the average thermal phonon lifetime, following a previous an-harmonic decay model. Experimental results obtained for cubic ice are in good agreement with the literature, indicat-ing the applicability of this anharmonic model by Maris in the ambiguous frequency range $\omega\tau_{ph} \sim 1$ and $\omega\tau_{ph} > 1$.

According to continuum elastic theory, the acoustic reflectivity of an interface is determined by the acoustic impedances of the media on both sides of this interface. For the acoustic wave incident from material A to material B, the reflectivity is expressed as [21]

$$R = \frac{Z_A - Z_B}{Z_A + Z_B}, \qquad (1)$$

where Z is the acoustic impedance of the medium. In a dissipative medium, the complex acoustic impedance will be a function of acoustic frequency and is given by [22]

$$Z(\omega) = \rho \frac{\omega}{k(\omega) + i\alpha(\omega)}, \qquad (2)$$

where ρ is the mass density, k is the acoustic wave number, and α is the acoustic attenuation constant in the medium. In the continuum elastic theory, k and α are related to the elastic constant, c, and viscosity coefficient, η, through [21]

$$k^2(\omega) = \frac{\rho\omega^2}{2c}\left(\frac{1}{\sqrt{1 + \omega^2\tau^2}} + \frac{1}{1 + \omega^2\tau^2}\right) \qquad (3)$$

and

$$\alpha^2(\omega) = \frac{\rho\omega^2}{2c}\left(\frac{1}{\sqrt{1 + \omega^2\tau^2}} - \frac{1}{1 + \omega^2\tau^2}\right), \qquad (4)$$

with $\tau = \eta/c$. In lossless media, $\eta = 0$, the acoustic im-pedance, $Z = \rho\omega/k = \rho v$, is a constant with a constant sound velocity v in the linear dispersion regime. In dis-sipative media, the dispersion relation, Eq. (3), will be modified by the viscosity coefficient, η, and the acoustic impedance will vary with frequency. From these equations, we can see that by measuring simultaneously the amplitude and the phase of the reflection, it is possible to obtain the acoustic wave number and the acoustic attenuation con-stant. To do so, we need to compare the amplitude and phase of waves reflected from the solid-solid interface and from the same surface and at the same location when the solid to be characterized is absent.

Two kinds of samples are used in this study [Fig. 1(a)]. For both samples, we first deposit an undoped c-axis GaN layer grown on a sapphire substrate. On one sample, we then grow a 3-nm-thick InGaN single quantum well (SQW), which allows the generation of broadband coher-ent acoustic phonon (CAP) pulse through the piezoelectric effect [13,15]. We then cap the SQW with a 70-nm-thick GaN layer. On the other sample, we grow a 10-period InGaN/GaN multiple quantum well (MQW) structure with a 150-nm GaN cap layer. The MQW structure enables
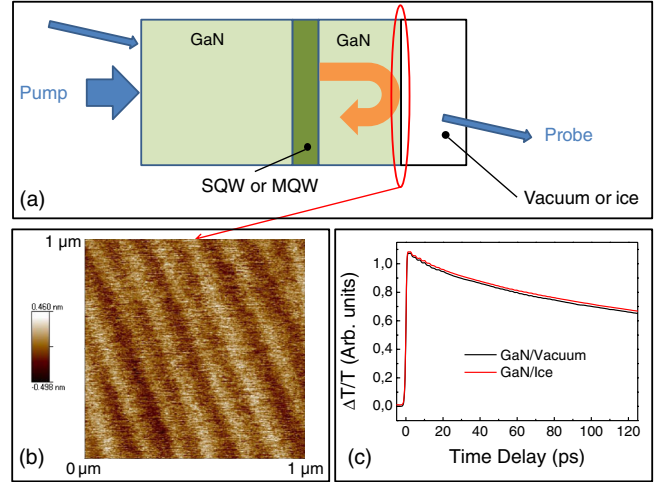

FIG. 1 (color online). (a) Schematic representation of the samples and experimental setup. (b) AFM image of the SQW sample GaN top surface. The rms roughness is $s = 0.12$ nm. (c) Transient transmission change obtained on the MQW sample with and without ice with a 400-nm wavelength for both pump and probe at 150 K.

the generation of quasimonochromatic CAP at a frequency given by the period of the structure [14].

To study the differences between the acoustic reflection at a free surface and at an interface, some precaution has to be taken to minimize the experimental uncertainties. First of all, we have to make sure of the quality of the surface, since surface roughness can induce scattering [13]. To estimate the loss due to surface roughness, we realized AFM imaging of the GaN top surface, which can be seen in Fig. 1(b). This image confirms the good quality of the surface, the root-mean-square roughness being $s =$ 0.12 nm. We thus do not expect the roughness to play a critical role [13]. Another issue concerns the possible modifications induced by the growth of a film on top of our sample. To minimize experimental error, we realized optical experiments *in situ*. The experimental procedure can be described as follows. The sample is placed inside the cryostat. We decrease the pressure to 10^{-4} Pa, and the temperature to 150 K, and a first experiment is realized, corresponding to a GaN − vacuum interface. We then create a small leak of air inside the chamber so that the pressure increases to 10^{-1} Pa without variation of the temperature. This will result in the formation of an ice layer on top of our sample. We maintain this pressure condition during one hour, and then we pump the chamber again. The growth conditions of the ice layer are similar to that of Ref. [23], so we expect to grow a few tens of nanometer thick cubic polycrystalline ice (Ic) layer. After the experiments, we monitored the pressure as a function of the temperature. A sudden rise of the pressure is observed at 220 K, which corresponds to the sublimation of ice at this pressure. Even though this procedure allows us to have a good control on the position where the experiments are

performed, we still need to dissociate the acoustic modifications from the optical ones engendered by the ice layer. The method used to make this separation is presented in the following.

The time-resolved experiments are carried on using a tunable Ti:sapphire oscillator and a conventional one-color pump and probe setup at normal incidence. The laser produces 100 fs optical pulses at a repetition rate of 76 MHz, centered at a wavelength tunable between 720 and 950 nm. Both pump and probe wavelengths are frequency doubled using a β-BaB$_2$O$_4$ (BBO) crystal. In all experiments, the pump and probe wavelengths are 400 nm. Figure 1(c) shows the transient transmission changes obtained on the MQW sample with and without ice. One first notes an initial increase of the transient transmission produced by photogenerated carriers on an ultrafast time scale. It is followed by a slow decrease due to electronic and thermal variation of the refractive index. After removing this background, by fitting with a double exponential decay, we obtained the traces reproduced in Fig. 2(a).

In Fig. 2(a), oscillations can be seen between 0 and 25 ps and between 40 and 90 ps. The first oscillation corresponds to the detection of the generated phonons propagating out of the MQW, while the latter one comes after reflection at the free surface or at the GaN − ice interface. In the following, we will refer to these oscillations as generation and echo signal, respectively. To analyze the differences between the acoustic reflections, we need to subtract the

optical effect of the ice layer. Thanks to the generation signal, it's possible to normalize both traces, so that the reflected echoes can be compared. By pumping on the back side of the sample, we can assume that the deposited energy in the MQW is the same with and without ice, and since the ice layer is really thin compared to the wavelength, Fabry-Perot effects can be neglected. In the inset of Fig. 2(a), we present the Fourier transform of the echo signal of both traces after normalization by the generation signal. On these Fourier transforms, two components can be clearly observed, one at 0.39 THz corresponding to the fundamental frequency generated by the MQW and a second one at 0.78 THz which is the second harmonic [24]. The modifications that are observed on the echo signal can now only be assigned to modification of the acoustic reflection caused by the ice layer. As expected, the reflection is weaker in the case of GaN − ice interface since the CAP is partially transmitted into the ice layer. We found the reflectivity to be $R_{0.39} = 0.71$ at 0.39 THz and $R_{0.78} = 0.61$ at 0.78 THz. The observed decrease of the reflectivity with increasing frequency is a clear effect of the modification of the acoustic impedance by the dissipative term η.

To complete our study, we realized experiments in the SQW sample. The SQW sample has the advantage of making the generation of broadband CAP possible [15]. In Fig. 2(b), we present the echo generated and detected by the SQW with and without ice. We can clearly see that the amplitude of the echo reflected from the GaN − ice interface is smaller. However, since only the echo can be detected, it is not possible to subtract the optical influence of the ice layer. But thanks to our MQW sample, we can normalize at 390 GHz.

Now that we have obtained the frequency spectra for SQW and MQW, we can obtain the amplitude and the phase of the complex reflection coefficient as depicted in Figs. 2(c) and 2(d). There are three material properties from Eqs. (1)–(4): mass density, ρ, elastic constant, c, and viscosity coefficient, η. We assume the mass density of ice to be a frequency-independent constant of 930 kg m^{-3} [23]. Concerning the properties of GaN, we take for the density 6095 kg m^{-3} [25], the sound velocity is obtained from the roundtrip time of the echo and is found to be 8000 ms^{-1}, and we consider that the viscosity in GaN is negligible. The other two quantities of ice can be determined by the complex reflection coefficient. According to the complex reflection coefficient at 0.39 THz obtained by using MQWs, the elastic constant, c, and viscosity coefficient, η, were found to be 11.6 GPa and 8.6×10^{-3} Pa s, respectively. The value that we obtain for the elastic constant corresponds to a longitudinal sound velocity of 3531 ms^{-1}, in good agreement with the literature [23,26]. From the elastic constants and the viscosity we obtained previously, we can calculate the reflection spectrum by using Eq. (1), as shown in Figs. 2(c) and 2(d). The excellent agreement between the calculated complex
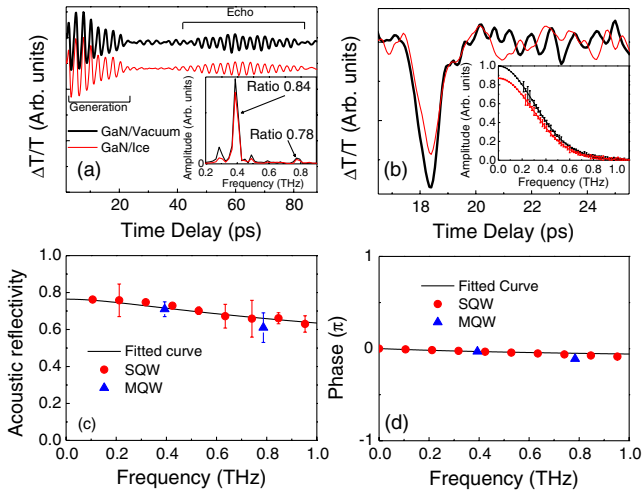

FIG. 2 (color online). (a) Transient transmission change in the MQW sample with and without ice at 150 K. Inset: Fourier transform of the reflected signal with and without ice, normalized by the generated signal. (b) Transient transmission change in the SQW sample with and without ice. Inset: Fourier transform of the reflected signal with and without ice, normalized by the 390 GHz signal from MQW. (c) Amplitude of the reflection coefficient of the GaN − Ice interface using MQW (triangle) and SQW (dots) sample and calculated using Eq. (1). (d) Phase of the reflection coefficient of the GaN − Ice interface using MQW (triangle) and SQW (dots) sample and calculated using Eq. (1).

reflection spectra and the one obtained by using SQW confirms the validity of the continuum elastic theory in the frequency range of 0.1 to 1 THz.

One notices, on Fig. 2(c), that the amplitude decreases at high frequency due to the modification of the impedance of ice caused by the absorption, meaning that phonons transmit more into ice. This phenomenon can be related to the Kapitza resistance. According to Ref. [2], the thermal boundary resistance can be approximated by

$$R_b T^3 = \left(\frac{\pi^2}{15} \frac{k_b^4}{\hbar^3} \sum_j c_{1,j} \Gamma_{1,j} \right)^{-1} \tag{5}$$

with

$$\Gamma_{1,j} = \int_0^{\pi/2} \alpha_{1 \to 2}(\theta, j) \cos(\theta) \sin(\theta) d\theta, \tag{6}$$

where $c_{1,j}$ is the phonon velocity in medium 1 of the phonon mode j, and $\alpha_{1 \to 2}(\theta, j)$ is the transmission probability of phonon mode j with incident angle θ. By applying this formula, we can obtain an estimated thermal boundary resistance that we reproduce in Fig. 3(a). The correspondence between phonon frequency and effective temperature is obtained by considering the frequency of the dominant phonon mode at a given temperature [2].

In this trace, the acoustic mismatch between GaN and ice as well as the effect of absorption are taken into account. However, since we compare the reflection from the GaN − vacuum and GaN − ice interfaces, the influence of the surface roughness cannot be seen. The thermal boundary resistance caused by the surface roughness of the interface is determined by considering the reflectivity spectrum due to the loss of coherence caused by the surface roughness of the surface (see Supplemental Material [27] and Ref. [13]) and then by applying Eq. (5). To obtain the complete Kapitza resistance, we add the effect of surface roughness. One can see that up to 0.1 THz, the thermal
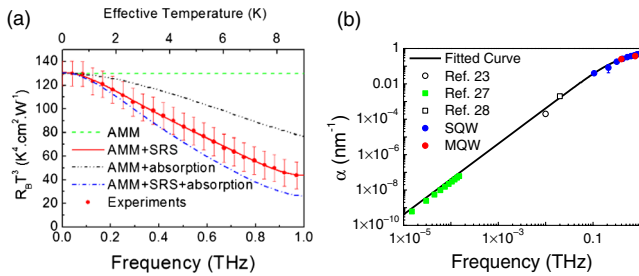

FIG. 3 (color online). (a) Thermal boundary resistance obtained by assuming that heat is carried by longitudinal acoustic phonons at normal incidence. Model based on acoustic mismatch, roughness, absorption, and a combination of these three effects are used and show that the absorption plays an important role in the sub-THz range. AMM denotes acoustic mismatch model, surface roughness scattering (SRS) roughness scattering. (b) Acoustic attenuation constant of cubic ice as a function of frequency.

boundary resistance is in pretty good agreement with the AMM, as expected [2]. At higher frequencies, the so-called Kapitza anomaly can be observed when the thermal boundary resistance decreases. This result demonstrates that the modification of the impedance caused by the absorption becomes non-negligible in the sub-THz range and can play a dominant role in the Kapitza anomaly. In other words, in this frequency range, the increase of the absorption modifies the acoustic impedance and thus reduces the mismatch, which leads to lower boundary resistance.

Another interesting aspect of this method is that we can get access to the THz attenuation spectrum by using Eq. (4). Figure 3(b) shows the attenuation constant as a function of the frequency. This acoustic attenuation constant is in good agreement with the value in the literature at lower frequency [23,28,29], and it is proportional to the frequency squared. At higher frequency (above 0.1 THz), the attenuation seems to saturate and does not follow the frequency squared trend. In this frequency range, the dominant attenuation mechanism is interaction with the thermal phonon bath. From the attenuation, we can obtain the thermal phonon lifetime in cubic ice [3],

$$\alpha(\omega, t) = \frac{C_v T}{2 \rho v_D^3} (\langle \gamma_{kj}^2 \rangle - \langle \gamma_{kj} \rangle^2) \frac{\omega^2 \tau_{ph}}{1 + \omega^2 \tau_{ph}^2}, \tag{7}$$

where C_v is the constant-volume heat capacity, T is the temperature, v_D is the average velocity for thermal phonons, γ_{kj} is the Grüneisen constant of thermal phonons with a wave vector k and a polarization j, and $\langle \cdots \rangle$ denotes an average over the thermal phonon spectrum. By fitting our results with this formula, we obtain a thermal phonon lifetime $\tau_{ph} = 0.2$ ps. In this case, our studied frequency range, 0.1–1 THz, corresponds to $\omega \tau_{ph} = 0.12$ to 1.2. We can compare this value to lifetime obtained from the kinetic formula of thermal conductivity κ,

$$\kappa = \frac{1}{3} C_v \langle v^2 \rangle \tau_{ph}, \tag{8}$$

where $\langle v^2 \rangle$ is the average of the squared velocity for thermal phonons. To obtain a simple estimate of the order of the phonon lifetime, we considered the velocity to be equal to the measured longitudinal sound velocity, 3500 ms^{-1}. Using 3.5 W m^{-1} K^{-1} for the thermal conductivity [30] and 3320 J kg^{-1} K^{-1} for the specific heat [31], we obtain a thermal phonon lifetime of 0.38 ps. The phonon lifetime can also be calculated using an approximated formula for the average sound velocity that takes into account transverse waves [32],

$$v = \left(\frac{1}{3} \left[\frac{2}{v_t^3} + \frac{1}{v_l^3} \right] \right)^{-(1/3)}, \tag{9}$$

where v_t and v_l are the transverse and longitudinal sound velocity. Using the elastic constants of Ref. [33], we obtain a lifetime of 0.75 ps, in the subpicosecond range, as our experimentally observed lifetime. Different mechanisms

could explain these discrepancies. First, thermal conductivity and attenuation often lead to differences [34], then the imperfection, such as defects in our sample, could reduce the lifetime. However, the agreement on the order of the lifetime shows that even though Eq. (7) by Maris was derived for the case $\omega\tau_{ph} \ll 1$, it can still quantitatively describe the acoustic attenuation behavior in the transition frequency regime between $\omega\tau_{ph} \ll 1$ and $\omega\tau_{ph} \gg 1$.

Measuring the thermal conductivity of ice could have importance for the study of interfacial water. Indeed, there are ongoing debates about whether the properties of water at an interface are more solid or waterlike [35]. Being able to measure the thermal conductivity of ice at this frequency will make the comparison with interfacial water, which has a usual thickness of around 1 nm, possible. Moreover, the thermal properties of ice are important due to its presence in solar system objects [36]. Furthermore, the method we present here is not limited to ice, but can already be applied to study the elastic and thermal properties at frequency up to 1 THz in an array of critical materials, like liquids, polymers, or biological tissues. And, by carefully designing the experimental setup [37,38], this technique can be applied to characterize materials in a deposition chamber.

————————

*sun@ntu.edu.tw

[1] G. Tas and H. J. Maris, Phys. Rev. B **55**, 1852 (1997).

[2] E. T. Swartz and R. O. Pohl, Rev. Mod. Phys. **61**, 605 (1989).

[3] H. J. Maris, in *Physical Acoustics*, Vol. 8, edited by W. P. Mason and R. Thurston (Academic, New York, 1971), p. 279.

[4] W. Chen, H. J. Maris, Z. R. Wasilewski, and S.-I. Tamura, Philos. Mag. B **70**, 687 (1994).

[5] A. A. Maznev, F. Hofmann, A. Jandl, K. Esfarjani, M. T. Bulsara, E. A. Fitzgerald, G. Chen, and K. A. Nelson, Appl. Phys. Lett. **102**, 041901 (2013).

[6] T.-M. Liu, S.-Z. Sun, C.-F. Chang, C.-C. Pan, G.-T. Chen, J.-I. Chyi, V. Gusev, and C.-K. Sun, Appl. Phys. Lett. **90**, 041902 (2007).

[7] R. Vacher, S. Ayrinhac, M. Foret, B. Rufflé, and E. Courtens, Phys. Rev. B **74**, 012203 (2006).

[8] P. Benassi, S. Caponi, R. Eramo, A. Fontana, A. Giugni, M. Nardone, M. Sampoli, and G. Viliani, Phys. Rev. B **71**, 172201 (2005).

[9] C. Masciovecchio, A. Gessini, S. Di Fonzo, L. Comez, S. C. Santucci, and D. Fioretto, Phys. Rev. Lett. **92**, 247401 (2004).

[10] C. Masciovecchio, G. Ruocco, F. Sette, P. Benassi, A. Cunsolo, M. Krisch, V. Mazzacurati, A. Mermet, G. Monaco, and R. Verbeni, Phys. Rev. B **55**, 8049 (1997).

[11] C. Thomsen, H. T. Grahn, H. J. Maris, and J. Tauc, Phys. Rev. B **34**, 4129 (1986).

[12] A. Devos, M. Foret, S. Ayrinhac, P. Emery, and B. Rufflé, Phys. Rev. B **77**, 100201 (2008).

[13] Y.-C. Wen, C.-L. Hsieh, K.-H. Lin, H.-P. Chen, S.-C. Chin, C.-L. Hsiao, Y.-T. Lin, C.-S. Chang, Y.-C. Chang, L.-W. Tu, and C.-K. Sun, Phys. Rev. Lett. **103**, 264301 (2009).

[14] C.-K. Sun, J.-C. Liang, and X.-Y. Yu, Phys. Rev. Lett. **84**, 179 (2000).

[15] Y.-C. Wen, S.-H. Guol, H.-P. Chen, J.-K. Sheu, and C.-K. Sun, Appl. Phys. Lett. **99**, 051913 (2011).

[16] P. Emery and A. Devos, Appl. Phys. Lett. **89**, 191904 (2006).

[17] T.-M. Liu, S.-Z. Sun, C.-F. Chang, G.-T. Chen, C.-C. Pan, J.-I. Chyi, and C.-K. Sun, Chin. J. Phys. (Taipei) **49**, 171 (2011).

[18] S. Ayrinhac, M. Foret, A. Devos, B. Rufflé, E. Courtens, and R. Vacher, Phys. Rev. B **83**, 014204 (2011).

[19] C. Klieber, E. Peronne, K. Katayama, J. Choi, M. Yamaguchi, T. Pezeril, and K. A. Nelson, Appl. Phys. Lett. **98**, 211908 (2011).

[20] K.-H. Lin, D.-H. Tsai, K.-J. Wang, S.-H. Chen, K.-L. Chi, J.-W. Shi, P.-C. Chen, and J.-K. Sheu, AIP Adv. **3**, 072126 (2013).

[21] D. Royer and E. Dieulesaint, *Elastic Waves in Solids I: Free and Guided Propagation*, Advanced Texts in Physics (Springer, New York, 2000).

[22] K. ichi Tozaki, M. Kimura, N. Komatsu, and S. Itou, Jpn. J. Appl. Phys. **31**, 2592 (1992).

[23] S. Kashiwada, O. Matsuda, J. J. Baumberg, R. L. Voti, and O. B. Wright, J. Appl. Phys. **100**, 073506 (2006).

[24] G.-W. Chern, K.-H. Lin, Y.-K. Huang, and C.-K. Sun, Phys. Rev. B **67**, 121303 (2003).

[25] A. Polian, M. Grimsditch, and I. Grzegory, J. Appl. Phys. **79**, 3343 (1996).

[26] W. Mason, *Physical Acoustics and the Properties of Solids*, The Bell Telephone Laboratories Series (Van Nostrand, Princeton, 1958).

[27] See Supplemental Material at http://link.aps.org/supplemental/10.1103/PhysRevLett.111.225901 for derivation of roughness induced reflection and details on Kapitza resistance.

[28] J. Tatibouet, R. Vassoille, and J. Perez, J. Glaciol. **15**, 161 (1975).

[29] Y.-C. Wen, C.-Y. Chen, K.-H. Lin, T.-F. Kao, Y.-R. Huang, and C.-K. Sun, in *Conference on Lasers and Electro-Optics/Quantum Electronics and Laser Science Conference and Photonic Applications Systems Technologies 2006 Technical Digest* (Optical Society of America, Washington, DC, 2006).

[30] O. Andersson and A. Inaba, Phys. Chem. Chem. Phys. **7**, 1441 (2005).

[31] A. Melinder, Int. J. Refrig. **33**, 1506 (2010).

[32] O. L. Anderson, J. Phys. Chem. Solids **24**, 909 (1963).

[33] V. P. Shpakov, J. S. Tse, V. R. Belosludov, and R. V. Belosludov, J. Phys. Condens. Matter **9**, 5853 (1997).

[34] R. O. Pohl, X. Liu, and E. Thompson, Rev. Mod. Phys. **74**, 991 (2002).

[35] J. W. M. Frenken and T. H. Oosterkamp, Nature (London) **464**, 38 (2010).

[36] R. M. Mastrapa, W. M. Grundy, and M. S. Gudipati, *Amorphous and Crystalline H2O-Ice* Astrophysics and Space Science Library (Springer, New York, 2013).

[37] A. Canillas, E. Bertran, J. Andujar, and J. Morenza, Vacuum **39**, 785 (1989).

[38] D. E. Aspnes, J. P. Harbison, A. A. Studna, and L. T. Florez, J. Vac. Sci. Technol. A **6**, 1327 (1988).